LAWRENCE
LIVERMORE
NATIONAL
LABORATORY

LLNL-TR-663385

Proton acceleration by relativistic self-guided laser pulses

Y. Chen, D. A. Alessi, R. Drachenberg, B. B. Pollock, F. Albert, J. E. Ralph, L. C. Haefner

October 29, 2014

Disclaimer

This work performed under the auspices of the U.S. Department of Energy by Lawrence Livermore National Laboratory under Contract DE-AC52-07NA27344.

Proton acceleration by relativistic self-guided laser pulses

Yu-hsin Chen, David Alessi, Derek Drachenberg, Bradley Pollock, Felicie Albert, Joseph Ralph, and Constantin Haefner

Lawrence Livermore National Laboratory, Livermore, California 94550, USA

October 16th, 2014

Abstract: Energetic protons and ions can be produced by the irradiation of a μm-thick solid target with an intense laser pulse via Target Normal Sheath Acceleration (TNSA). Typically the maximum proton energy increases with decreasing target thickness. However, amplified spontaneous emission (ASE) from the drive laser system may alter thinner targets before arrival of the main pulse and limit the attainable proton energy. Here we experimentally test a method of reducing ASE intensity and increasing TNSA proton energy by using relativistic self-guiding in an underdense plasma.

INTRODUCTION

Target normal sheath acceleration

The advance of high intensity laser technologies in the recent years has enabled access to laser-plasma interactions in the relativistic regime. Production of energetic protons and ions by irradiating an intense ($> 10^{19}$ W/cm^2) laser pulse onto a thin solid target is of particular interest to many research groups. The laser-driven proton/ion source is a promising candidate to replace the conventional radio frequency (RF) accelerator due to its extremely high acceleration gradient (~

10^{12} eV/m) and compact footprint. Potential applications of laser-based proton source include, proton radiography [1], probing field structures of high-density plasmas [2], creating warm dense matters via isochoric heating [3], and proton therapy [4]. The best-known acceleration mechanism is target normal sheath acceleration (TNSA) [5, 6]. In TNSA, an intense laser pulse is focused onto the front surface of a hydrocarbon-coated thin (a few μm to sub-μm) target and produces hot electrons within the focal area. The hot electrons (typically a few MeV) then penetrate and leave the target to form a "sheath" above the rear surface. The charge separation then creates a strong quasi-static field that accelerates ions and protons at the rear surface.

A typical TNSA ion spectrum has a Boltzmann-like distribution with a cutoff energy. In principle, the cutoff (maximum) ion energy tends to increase when reducing the target thickness, owing to the following reasons. First, the hot electrons have a certain transverse spread when traverse across the target. Therefore a thicker target may lead to lower electron density in the sheath at its back surface, which reduces the acceleration field. Also the hot electrons may lose their energy in the target due to collisions. In addition, the effect of hot electron recirculation is more significant for the thin target, which increases the sheath electron density and thus enhances the acceleration.

The effect of laser temporal contrast

However, after taking the temporal contrast of the TNSA-driving laser pulse into consideration, the aforementioned energy scaling with respect to the thickness does not always hold. For short pulse laser systems with intensities ($> 10^{19}$ W/cm^2) sufficient to accelerate protons to above MeV level, a common problem is the amplified spontaneous emission (ASE). The ~ ns-long ASE pedestal may well exceed ~ $10^{11} - 10^{12}$ W/cm^2 at the target surface and result

to ionization. The ablation pressure then launches a shock wave that propagates across the target. Depending on the target material, thickness, as well as intensity and duration of the prepulse, the shock wave may deform or blowout the back surface of the target before the main pulse arrives [7]. The reduced density gradient at the back surface may decrease the sheath field from $\sim T_e / e\lambda_D$ to $\sim T_e / eL_{ss}$ and thus degrade the ion acceleration, where the plasma scale length L_{ss} is much greater than the Debye length λ_D due to early ionization and expansion [8]. For instance, with a sufficiently low laser prepulse intensity ($\sim < 10^{10}$ W/cm^2), Mackinnon *et el*. observed that the TNSA proton cutoff energy is increased from 8 to 24 MeV when the thickness of the aluminum target is reduced from 10 to 3 μm at 10^{20} W/cm^2 laser peak intensity [9]. On the other hand, Kaluza *et al*. reported that with the presence of a $\sim 5 \times 10^{11}$ W/cm^2 ASE pedestal, the maximum attainable proton energy is peaked at an optimal target thickness. The optimal thickness is increased from 2 to 10 μm with deteriorated peak proton energy when the prepulse duration is increased from 0.5 to 2.5 ns [10].

Therefore to enhance TNSA by reducing the target thickness, it is required to suppress the laser prepulse intensity. The high temporal laser contrast ($> 10^9 - 10^{10}$) favored by TNSA process is generally not achievable without careful laser system design along with series of sophisticated pulse cleaning techniques. The examples include cross-polarized wave generation (XPW) [11], nonlinear elliptical rotation [12], fast saturable absorbers [13], and Pockels cells, in conjunction with system architectures such as double CPA [14] and pre-amplification of short pulse [13]. Another approach is to enhance the contrast at the "target side", such as plasma mirrors [15]. It has become a popular technique in the recent years; however it requires extra high-cost optics, is not trivial to align and is not suitable for high-rep-rate operation owing to contamination by solid debris. Here we experimentally investigate an alternate contrast

enhancement method using relativistic self-guiding [16] of the intense laser pulse in the underdense plasma. The idea is first proposed by Sprangle *et al*. in 1991 [17], but to our best knowledge there is no experimental demonstration so far. In our experiment, the plasma is produced in a back-filled gas cell, which is low-cost, debris-free, and can be operated at higher rep rate (> 10 Hz) for potential applications requiring high average flux. Realizing the sensitivity of the maximum accelerated proton energy to the laser prepulse, we choose TNSA protons as an indicator for evaluating the feasibility of this technique, and it could also apply to other laser-solid experiments that require ultrahigh contrast.

RELATIVISTIC SELF-GUIDING AND ITS APPLICATION TO LASER CONTRAST ENHANCEMENT

Relativistic self-guiding is a nonlinear propagation phenomenon when the laser exceeds the critical power $P_{cr} = 17\omega^2 / \omega_p^2$ GW in the plasma [18], in which the laser pulse can maintain high intensity with tightly-confined transverse profile over multiple Rayleigh lengths z_R. An important application in recent years is the laser wakefield acceleration of electrons [19]. By self-guiding the laser pulse in the underdense plasma, it is possible to drive the wakefield in the highly nonlinear ("blowout" or "bubble") regime over a few mm to ~ 1 cm, and electron energy up to ~ 1 GeV was observed [20]. The phenomenon of self-guiding originates from (1) intensity-dependent plasma frequency due to relativistic modification of electron mass $\omega_p = \sqrt{4\pi n_e e^2 / \gamma m_e}$, where $\gamma = \sqrt{1 + a_0^2 / 2}$ is the Lorentz factor and

$a_0 = \sqrt{I[\mathrm{W/cm^2}](\lambda[\mu\mathrm{m}])^2 / 1.37 \times 10^{18}}$ is the normalized vector potential, as well as (2) cavitation of electron plasma by the ponderomotive force [21].

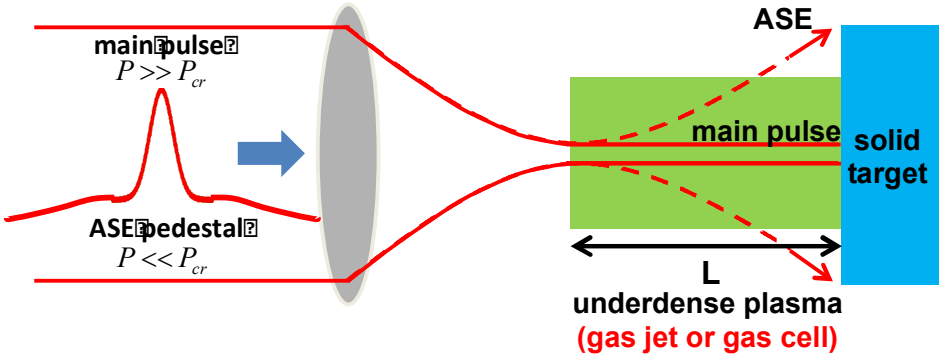

Fig. 1. Laser contrast enhancement using relativistic self-guiding in the plasma.

As illustrated in Fig. 1, our proposed contrast enhancement method relies on the fact that the power of the laser prepulse is generally orders of magnitude lower than P_{cr}. The laser pulse is focused at the front edge of the underdense plasma, immediately followed by the TNSA solid target. By properly choosing the f-number of the focusing optics and the plasma length, it is possible to guide the main laser pulse with $P > P_{cr}$ for a distance $z >> z_R$ in the plasma while maintaining its relativistic intensity until reaching the solid target, while the ASE prepulse intensity is reduced due to natural diffraction. The ASE attenuation factor is given by $\sim (z / z_R)^2$ assuming $z >> z_R$.

The intense laser pulse encounters energy loss while being guided through the plasma. For the application of ion acceleration, the required laser intensity is > 10^{19} W/cm^2. Moreover, the pulse duration of the laser system (Callisto, detail will be described later) we used in the experiment is sub-100 fs. The nonlinear propagation of such laser pulse in the plasma is typically in the bubble regime, where the laser pulse is guided within a co-moving cavitation structure of

electron plasma driven by the ponderomotive force, accompanied by production of large-amplitude wakefields. For optimal self-guiding with minimal energy loss, the laser and the plasma parameters have to meet certain criteria. First of all, the pulse length should be roughly equal to the plasma wavenumber ($c\tau \sim k_p$). In addition, the laser vacuum spot size w_0 (1/e field radius) must match the blowout radius of electrons $R_b = \sqrt{a_0} / k_p$ [22]. Initially unmatched laser spot causes energy loss through diffraction when propagating in the plasma. Figure 2 shows the plasma density vs. laser intensity satisfying the matching condition at various spot sizes with λ = 800 nm. Another important loss mechanism is the energy transfer to the plasma wake via "etching" at the pulse rising edge. A characteristic pump depletion length $L_{pd} = (\omega^2 / \omega_p^2) c\tau$ is used to estimate the propagation length over which the whole laser pulse is fully etched, and the expression is valid for $2 < a_0 < 20$ [22]. For our purpose of attenuating the prepulse while maintaining sufficiently high intensity/energy of the main pulse for TNSA, the plasma length L must satisfy the following two criteria: (1) $L >> \pi w_0^2 / \lambda$ (Rayleigh length) so that the intensity of un-guided prepulse can be sufficiently attenuated by diffraction, and (2) $L << L_{pd}$ for preventing significant laser energy loss due to driving the wakefield. Calculated L_{pd} vs. electron density with pulse duration ranging from 50 to 100 fs is shown in Fig. 3. Owing to the difficulty of directly measuring the laser contrast at the end of the self-guiding in the plasma, here we use TNSA process with various solid target thicknesses to benchmark the contrast improvement.

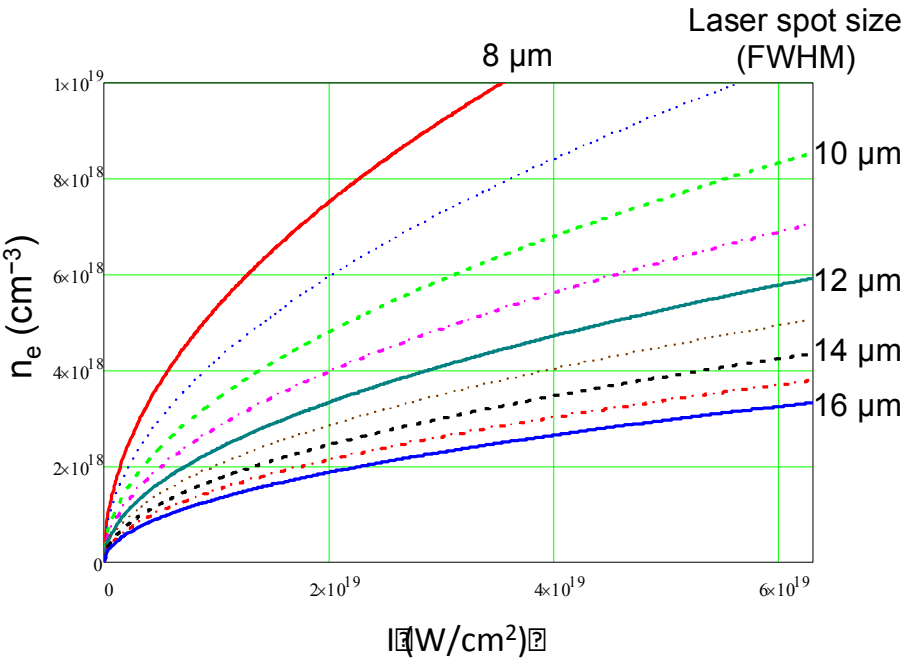

Fig. 2. Calculated laser intensity and plasma density satisfying the matching condition at various laser spot FWHM sizes. The laser wavelength is 800 nm.

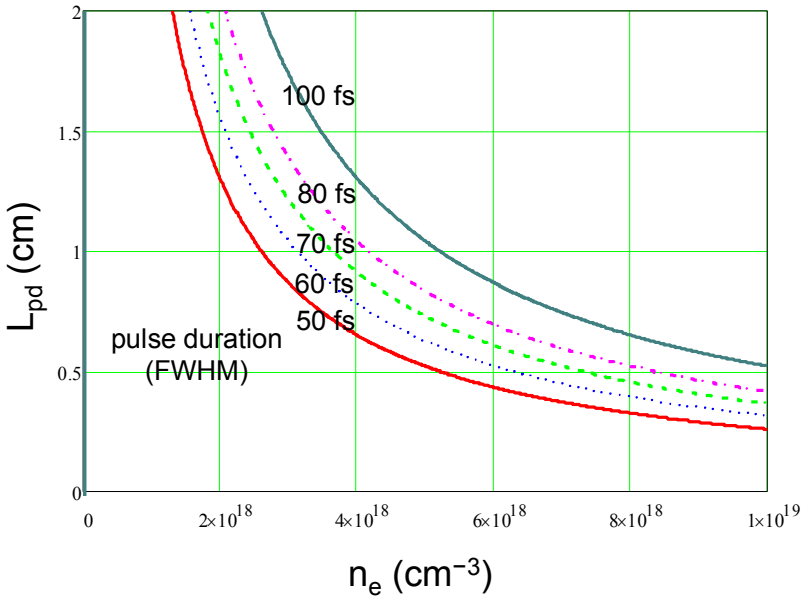

Fig. 3. Pump depletion length vs. plasma density at various laser pulse durations, calculated at $\lambda = 800$ nm.

EXPERIMENT

The experiment was conducted using Callisto laser at Jupiter Laser Facility, Lawrence Livermore National Laboratory. Callisto is a single-shot (~ 30 minute/shot), Ti:Sapphire laser system with ~ 80 fs pulse duration and 12 J maximum energy. An f/8 off-axis parabola (OAP) was used to focus the laser beam to a ~ 11 μm FWHM spot containing ~ 40% of laser energy. The laser contrast is measured by a fast photodiode and is shown in Fig. 4. The combined measurement system (phototiode, cable, oscilloscope) gives a ~ 100 ps signal rise time. The normalized prepulse intensity is ~ 10^{-9} at −1.2 ns and is rapidly increased to ~ 10^{-5} near 0 ns.

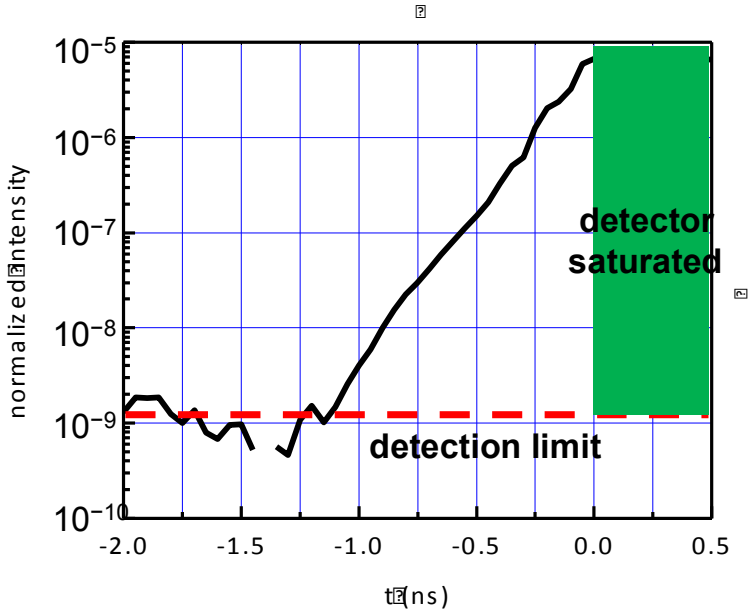

Fig. 4. Callisto laser contrast measured by a fast photodiode.

The experimental setup is shown in Fig. 5. The laser is focused at the 100-μm-diameter entrance pinhole of a gas cell backfilled with helium. The rising edge of the laser pulse ionizes the helium, producing plasma with density range 10^{18} – 10^{19} cm^{-3}, variable by adjusting the backing pressure. The plasma density n_e is determined by interferometry with a ~ 100-fs-duration

probe beam transversely passing through the fused silica sidewalls of the cell. An aluminum target foil is mounted on a holder sealing the end of the cell, with 15° angle of incidence with respect to the laser propagation. A Thomson parabola (TP) with similar design to Ref. [23] is placed ~ 6 cm away from the target at the normal direction. A Fujifilm imaging plate covered by 6-μm-thick, Al-coated mylar foil is used to detect protons. A stack of radiochromic films (RCF) wrapped by 15-μm-thick Al foil, with a 6-mm aperture cut at the center, is placed immediately before the pinhole of TP. This is to measure the energy-dependent proton beam profile, as well as to ensure the center portion of the proton beam is sampled by TP.

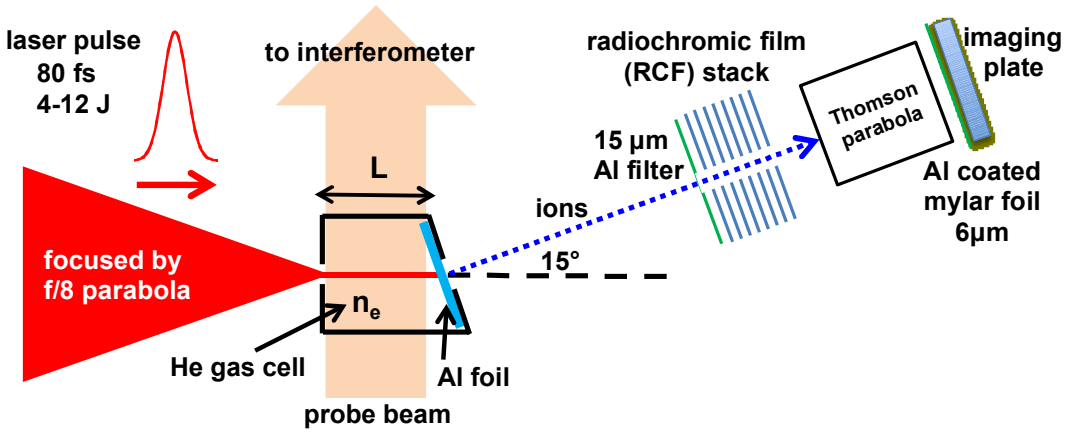

Fig. 5. Experimental setup.

During our experimental campaign, Callisto output energy has significant shot-to-shot fluctuation (~ 4 − 12 J), which makes it difficult to select n_e value exactly satisfying the matching condition according to Fig. 2. Here we choose $n_e \sim 5 \times 10^{18}$ cm^{-3} corresponding to the averaged laser energy ~ 8 J (peak intensity ~ 3×10^{19} W/cm^2). This also gives the pump depletion length L_{pd} ~ 8.3 mm from Fig. 3, and then the gas cell length L can be determined. From the contrast measurement in Fig. 4, the prepulse intensity ~ 10^{12} W/cm^2 is sufficient to ionize the target surface. To prevent pre-ionization, it is preferable to suppress the prepulse

intensity by at least a factor of 100, which gives L = 3.7 cm while satisfying the requirement of $L << L_{pd}$.

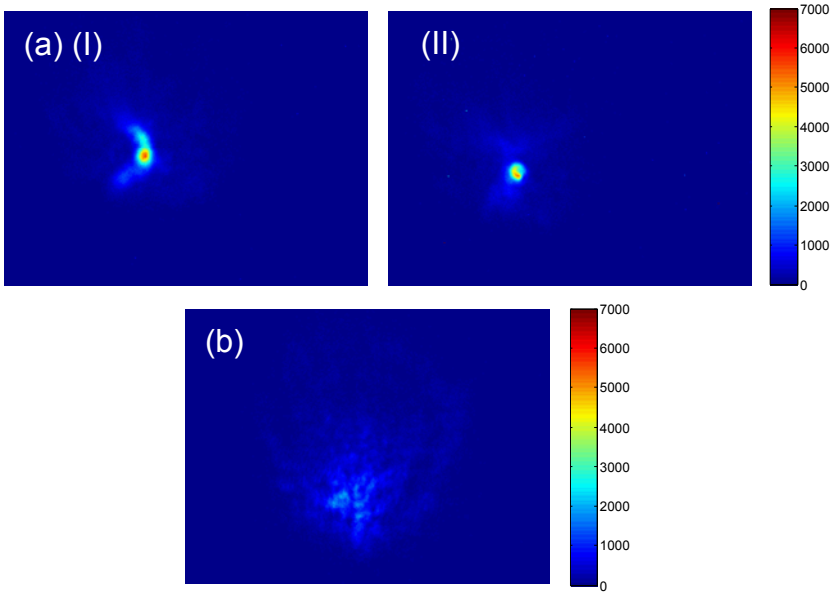

Fig. 6. Typical laser spot profiles at the exit of the gas cell (a) with and (b) without the plasma. The plasma density is 3.5×10^{18} cm^{-3} and 5.5×10^{18} cm^{-3} in (a)(I) and (a)(II), respectively.

We first investigated self-guiding by measuring the laser profile at the exit of the plasma. The target holder at the end of the gas cell is replaced by a 1-mm-diameter exit pinhole, and the laser spot at the pinhole is imaged onto a CCD camera through a pair of relaying lenses and a microscope objective. Within the imaging system, surface reflections from wedges and Kodak Wratten filters are used to achieve proper attenuation for the CCD camera. Figure 6(a) and 6(b) show typical laser spot images at the exit pinhole with and without plasma, respectively. Without plasma the laser propagates in the vacuum for 3.7 mm after focus, and the FWHM beam diameter is expanded to ~ 200 μm. When plasma is present ($n_e \sim 3.5 \times 10^{18}$ cm^{-3} in Fig. 6(a)(I) and ~ 5.5×10^{18} cm^{-3} in Fig. 6(a)(II)), a ~ 40-μm-diameter spot surrounded by low-intensity halo is observed. This indicates that the laser pulse is self-guided in the plasma, with a portion of

energy leaving the guided spot by continuous diffraction during propagation. It is estimated that ~ 60% of transmitted laser energy is within the spot at the end of guiding. The measurement was performed at various plasma densities, and we found that, while we are not able to eliminate the un-guided halo, optimal guiding is achieved within the range of $n_e \sim 3.5 - 5.5 \times 10^{18}$ cm^{-3}, which agrees reasonably well with the matched spot condition given in Fig. 2.

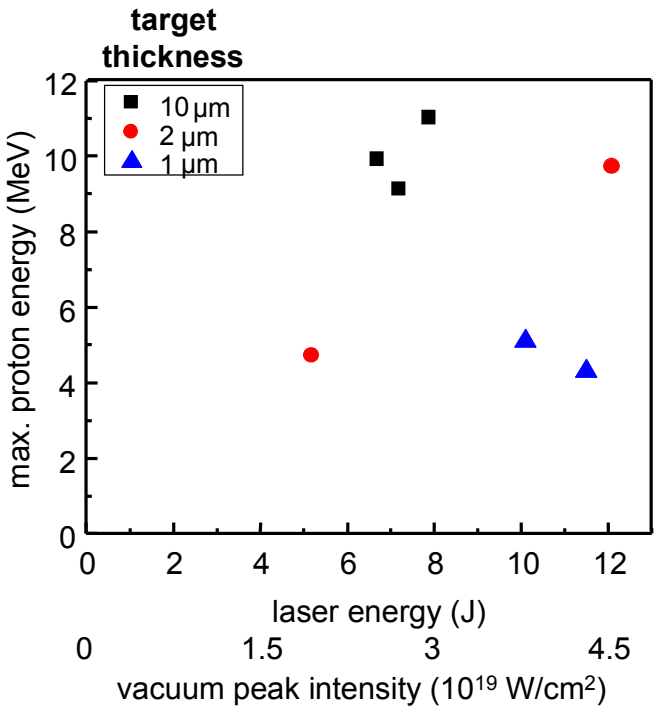

Fig. 7. Maximum (cutoff) proton energy vs. laser pulse energy with Al target thicknesses 10 μm, 2 μm, and 1 μm. The laser is directly focused onto the target surface in vacuum.

After obtaining the optimal parameters for self-guiding, we conducted two series of proton acceleration experiments. For comparison, we first produced TNSA protons without self-guiding, i.e., directly focusing the laser onto the target front surface in vacuum. Three different Al target thicknesses (10, 2, and 1 μm) are used, and the maximum proton energy recorded by TP with respect to laser pulse energy is shown in Fig. 7. Note that although we are not able to

directly compare the maximum proton energy vs. target thickness at the same laser energy, the data points in Fig. 7 form three distinct slopes, and each corresponds to different target thickness. It can be seen that the 10 μm target has best acceleration efficiency in terms of maximum proton energy as the function of incident laser energy, and the 1 μm target is the worst. This can be explained by the results of contrast measurement shown in Fig. 4: the prepulse intensity reaches ~ 4.5×10^{12} W/cm^2 at − 500 ps (contrast ~ 6.7×10^6 with peak intensity ~ 3×10^{19} W/cm^2), and the ablation pressure launches a shock wave at a speed ~ 10 μm/ns across the Al target [7]. The shock travels ~ 5 μm before the main pulse arrives, and therefore for a 10 μm target, the back surface will be intact for the main pulse driving TNSA process.

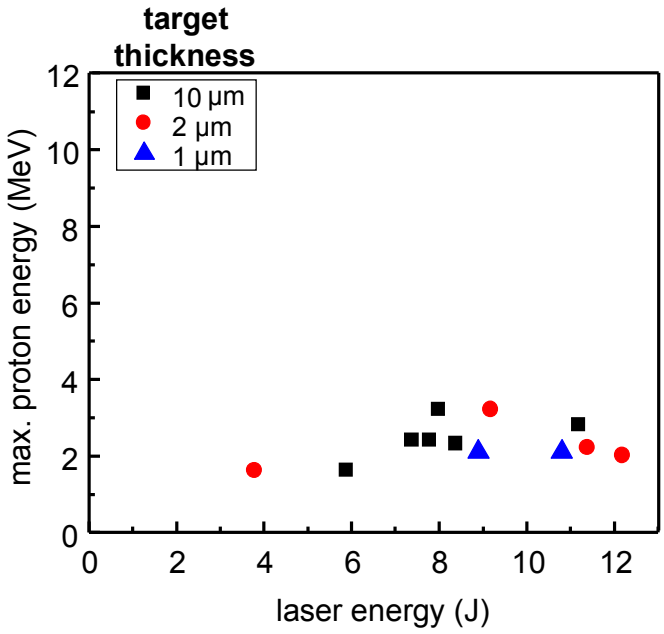

Fig. 8. Maximum (cutoff) proton energy vs. laser pulse energy with Al target thicknesses 10 μm, 2 μm, and 1 μm. The laser pulse is self-guided over 3.7 mm in the plasma ($n_e = 5 \times 10^{18}$ cm^{-3}) before reaching the target surface.

Finally we employed self-guided laser pulses for TNSA experiment, with the same Al target thicknesses previously used. Before reaching the target, the laser pulse is first self-guided for ~ 3.7 mm in the plasma with $n_e \sim 5 \times 10^{18}$ cm^{-3}, and the maximum proton energy with

respect to initial laser energy is shown in Fig. 8, with two interesting features: In contrast to un-guided laser-driven TNSA, the proton cutoff energy (1) has much weaker dependence on the input laser energy, and (2) is not affected by the target thickness. Feature (1) indicates that the laser peak intensity reaching the target front surface remains roughly the same when varying the input laser energy between 4 – 12 J. Moreover, feature (2) may be the indication of partially reduced laser prepulse intensity – it may be in the regime that the effect of reduced density gradient by the shock wave at the target back surface is canceled by the enhancement of sheath electron density when decreasing the target thickness. Further investigations including simulations are required to identify underlying mechanisms and to explain these observations.

For all target thicknesses used in the experiment, the proton energies produced by guided laser pulse are much lower compared with those shown in Fig. 6. This is probably due to significant loss of laser energy in the plasma before reaching the solid target, indicating that the self-guiding is still not optimized. The authors note that due to the single-shot operation and large shot-to-shot laser energy fluctuation (> 100%) of the Callisto laser, the parameter scanning and optimization are extremely difficult. For future experimental works, a stable laser system is of utmost importance.

CONCLUSION

We have tested a novel method to enhance laser contrast as well as TNSA using an intense laser pulse self-guiding through an underdense plasma. This technique is relatively simple with lower cost, and is suitable for high rep rate laser operation. By comparing between the TNSA proton energies from un-guided and guided laser pulses at different target thicknesses, we observed features that may result from reduced prepulse intensity. Further investigations are required to better understand our observations and to optimize the process for applications of high-contrast laser-plasma experiments.

ACKNOWEDGEMENT

The authors thank S. Maricle for technical assistance and laser operation. This work was supported by LLNL's Laboratory Directed Research and Development Program LDRD-13-FS-006. This work was performed under the auspices of the U.S. Department of Energy by Lawrence Livermore National Laboratory under Contract DE-AC52-07NA27344.

REFERENCES

[1] A. J. Mackinnon, P. K. Patel, M. Borghesi, R. C. Clarke, R. R. Freeman, H. Habara, S. P. Hatchett, D. Hey, D. G. Hicks, S. Kar, *et al*., "Proton Radiography of a Laser-Driven Implosion," Phys. Rev. Lett. **97**, 045001 (2006).

[2] C. K. Li, F. H. Séguin, J. A. Frenje, J. R. Rygg, R. D. Petrasso, R. P. J. Town, P. A. Amendt, S. P. Hatchett, O. L. Landen, A. J. Mackinnon, *et al*., "Measuring E and B Fields in Laser-Produced Plasmas with Monoenergetic Proton Radiography," Phys. Rev. Lett. **97**, 135003 (2006).

[3] P. K. Patel, A. J. Mackinnon, M. H. Key, T. E. Cowan, M. E. Foord, M. Allen, D. F. Price, H. Ruhl, P. T. Springer, and R. Stephens, "Isochoric Heating of Solid-Density Matter with an Ultrafast Proton Beam," Phys. Rev Lett. **91**, 125004 (2003).

[4] V. Malka, J. Faure, Y. A. Gauduel, E. Lefebvre, A. Rousse, and K. T. Phuoc, "Principles and applications of compact laser-plasma accelerators," Nature Phys. **4**, 447 (2008).

[5] R. A. Snavely, M. H. Key, S. P. Hatchett, T. E. Cowan, M. Roth, T. W. Phillips, M. A. Stoyer, E. A. Henry, T. C. Sangster, M. S. Singh, *et al*., "Intense High-Energy Proton Beams from Petawatt-Laser Irradiation of Solids," Phys. Rev. Lett. **85**, 2945 (2000).

[6] S. C. Wilks, A. B. Langdon, T. E. Cowan, M. Roth, M. Singh, S. Hatchett, M. H. Key, D. Pennington, A. MacKinnon, and R. A. Snavely, "Energetic proton generation in ultra-intense laser-solid interactions," Phys. Plasmas **8**, 542 (2001).

[7] D. Batani, R. Jafer, M. Veltcheva, R. Dezulian, O. Lundh, F. Lindau, A. Persson, K. Osvay, C.-G. Wahlström, D. C. Carroll, P. McKenna, A. Flacco, and V. Malka, "Effects of laser prepulses on laser-induced proton generation," New J. Phys. **12**, 045018 (2010).

[8] H. Daido, M. Nishiuchi, and A. S. Pirozhkov, "Review of laser-driven ion sources and their applications," Rep. Prog. Phys. **75**, 056401 (2012).

[9] A. J. Mackinnon, Y. Sentoku, P. K. Patel, D. W. Price, S. Hatchett, M. H. Key, C. Andersen, R. Snavely, and R. R. Freeman, "Enhancement of Proton Acceleration by Hot-Electron Recirculation in Thin Foils Irradiated by Ultraintense Laser Pulses," Phys. Rev. Lett. **88**, 215006 (2002).

[10] M. Kaluza, J. Schreiber, M. I. K. Santala, G. D. Tsakiris, K. Eidmann, J. Meyer-ter-Vehn, and K. J. Witte, "Influence of the Laser Prepulse on Proton Acceleration in Thin-Foil Experiments," Phys. Rev. Lett. **93**, 045003 (2004).

[11] N. Minkovski, S. M. Saltiel, G. I. Petrov, O. Albert, and J. Etchepare, "Polarization rotation induced by cascaded third-order processes," Opt. Lett. **27**, 2025 (2002).

[12] R. W. Boyd, Nonlinear Optics, Academic Press (1992).

[13] M. Nantel, J. Itatani, An-Chun Tien, J. Faure, D. Kaplan, M. Bouvier, T. Buma, P. Van Rompay, J. Nees, P. P. Pronko, D. Umstadter, and G. A. Mourou, "Temporal Contrast in Ti:Sapphire Lasers: Characterization and Control," IEEE J. Sel. Topics Quantum Electron. **4**, 449 (1998).

[14] M. P. Kalashnikov, E. Risse, H. Schönnagel, and W. Sandner, "Double chirped-pulse-amplification laser: a way to clean pulses temporally," Opt. Lett. **30**, 923 (2005).

[15] C. Thaury, F. Quéré, J.-P. Geindre, A. Levy, T. Ceccotti, P. Monot, M. Bougeard, F. Réau, P. d'Oliveira, P. Audebert, R. Marjoribanks, and Ph. Martin, "Plasma mirrors for ultrahigh-intensity optics," Nature Phys. **3**, 424 (2007).

[16] E. Esarey and P. Sprangle, "Overview of Plasma-Based Accelerator Concepts," IEEE Trans. Plasma Sci. **24**, 252 (1996).

[17] P. Sprangle, A. Zigler, and E. Esarey, "Elimination of laser prepulse by relativistic guiding in a plasma," Appl. Phys. Lett. **58**, 346 (1991).

[18] Guo-Zheng Sun, Edward Ott, Y. C. Lee, and Parvez Guzdar, "Self-focusing of short intense pulses in plasmas," Phys. Fluids **30**, 526 (1987).

[19] T. Tajima and J. M. Dawson, "Laser Electron Accelerator," Phys. Rev. Lett. **43**, 267 (1979).

[20] C. E. Clayton, J. E. Ralph, F. Albert, R. A. Fonseca, S. H. Glenzer, C. Joshi, W. Lu, K. A. Marsh, S. F. Martins, W. B. Mori, A. Pak, F. S. Tsung, B. B. Pollock, J. S. Ross, L. O. Silva, and D. H. Froula, "Self-Guided Laser Wakefield Acceleration beyond 1 GeV Using Ionization-Induced Injection," Phys. Rev. Lett. **105**, 105003 (2010).

[21] J. E. Ralph, K. A. Marsh, A. E. Pak, W. Lu, C. E. Clayton, F. Fang, W. B. Mori, and C. Joshi, "Self-Guiding of Ultrashort, Relativistically Intense Laser Pulses through Underdense Plasmas in the Blowout Regime," Phys. Rev. Lett. **102**, 175003 (2009).

[22] W. Lu, M. Tzoufras, C. Joshi, F. S. Tsung, W. B. Mori, J. Vieira, R. A. Fonseca, and L. O. Silva, "Generating multi-GeV electron bunches using single stage laser wakefield acceleration in a 3D nonlinear regime," Phys. Rev. ST Accel. Beams **10**, 061301 (2007).

[23] D.C. Carroll, P. Brummitt, D. Neely, F. Lindau, O. Lundh, C.-G. Wahlström, and P. McKenna, "A modified Thomson parabola spectrometer for high resolution multi-MeV ion measurements—Application to laser-driven ion acceleration," Nucl. Instrum. Meth. A **620**, 23 (2010).